RSC Advances

ROYAL SOCIETY OF CHEMISTRY

www.rsc.org/advances

RSC Advances

ARTICLE

Catalyst free synthesis of three dimensional nanoworms like gallium oxide - graphene nanosheets hybrid structure with enhanced optical properties

Received 00th November 2015,
Accepted 00th December 2015

DOI: 10.1039/x0xx00000x

www.rsc.org/

Rajesh Kumar [a], Pawan Kumar Dubey [b], Rajesh Kumar Singh [c], Alfredo R. Vaz [a] and Stanislav A. Moshkalev [a]

We here report the synthesis and growth of catalyst free three dimensional beta-gallium oxide nanoworms like nanostructures on graphene nanosheets (3D β-Ga_2O_3@GNSs) using a solid mixture of graphite oxide and gallium acetylacetonate by microwave (MW) assisted method for the first time. The MW-assisted synthesis of 3D β-Ga_2O_3@GNSs hybrids contains 1D semiconducting β-Ga_2O_3 nanoworms (NWs) and 2D highly conducting graphene nanosheets (GNSs) materials. The β-Ga_2O_3 NWs have an average diameter of 200 nm and lengths of up to ~1 µm grown on the GNSs. These 3D β-Ga_2O_3@GNSs hybrids have been synthesized in very short time with scalable amount. The controlling parameters as MW irradiation time and power were found to greatly influence the structural morphology of as synthesized 3D β-Ga_2O_3@GNSs hybrid. This method for the synthesis of 3D β-Ga_2O_3@GNSs hybrids is imperative due to excellent control over experimental parameters, low cost and better reproducibility. Also, catalyst-free MW-assisted method is a much more rapid and thus higher throughput alternative for the effective and scalable growth over conventional heating method. The crystallinity, structure, morphology, and optical analysis of 3D β-Ga_2O_3@GNSs hybrids are carried out utilizing several techniques. The formation of 3D β-Ga_2O_3@GNss hybrids shows the band gap variation from 4.94 to 4.48 eV allied with the structural evolution. A suitable growth mechanism has been suggested for the formation of these 3D β-Ga_2O_3@GNSs hybrids.

Introduction

Three dimensional (3D) nanostructured materials are a focused research field both due to their importance in mesoscopic physics study and the increasing desire for implications of nano devices. The combinations of two different types of nanomaterials containing different dimensions make their properties attractive for the electron transportation from one side to other side with the help of their unique hybrids nanostructure. These type of hybrids nanostructure can be structured by one-dimensional growth of semiconducting nanomaterials (nanorods, nanowires and nanotubes) on two-dimensional carbon based materials like graphene nanosheets (GNSs). These 3D nanostructures have attracted much attention due to their novel importance in understanding fundamental physical concepts and potential applications in building blocks for electronic, thermal and optical nano-devices [1-3]. Gallium (Ga) based compound materials such as gallium nitride (GaN) [4], gallium oxynitride (GaON) [5], and gallium oxide (Ga_2O_3) [6] are among the promising inorganic semiconductors compound that provide numerous advantages over other organic materials for electronic and optoelectronic device applications [7-13]. Among above Ga based compound, the Ga_2O_3 possess different crystalline phases, including α-, β-, γ-, δ- and ε-Ga_2O_3 [14]. Among these phases, the monoclinic structured β-Ga_2O_3 is the most stable form, which is a UV transparent semiconductor with a wide band gap of 4.9 eV [15]. Ga_2O_3 also exhibits conduction and luminescence properties, and thus has potential applications in water splitting [16, 17], photocatalysis [18, 19], gas sensing [20, 21], nano-photonics [22], tunable phosphorescence [23] and plasmonic applications [24] etc. However, for the various applications purpose the Ga_2O_3 nanostructures have been synthesized by various methods, including laser ablation [25], arc-discharge [26], physical deposition via vapor-solid [27, 28], vapor-liquid-solid method [29] and so on. But the above mentioned synthesis methods, it is possible to synthesized only Ga_2O_3 nanostructures and no other binary elements presents.

The graphene reveals high theoretical surface area (2600 $m^2 g^{-1}$) [30], excellent thermal conductivity (4840-5300 W $m^{-1} K^{-1}$) [31], extremely high mechanical stiffness (tensile strength up to 130 GPa, modulus of 1000 GPa) [32], ultrahigh electron mobilities (2×10^5 $cm^2 V^{-1} s^{-1}$) [33, 34] due to its sp^2 hybridization with one-atom thick and two-dimensional honeycomb lattice structure. These properties

[a] Centre for Semiconductor Components, State University of Campinas (UNICAMP), 1308-870 Campinas, Sao Paulo, Brazil.
[b] Nanotechnology Application Centre, University of Allahabad, Allahabad 211002, India.
[c] Department of Physics, Indian Institute of Technology (Banaras Hindu University), Varanasi-221005, India.

make it to be one of the most fascinating and peculiar materials for the preparation of high performance hybrids with other functional inorganic semiconductors nanostructures [35]. These hybrid nanostructures of inorganic semiconductor and graphene can offer additional flexibility, functionality and novelty for realizing advanced optoelectronic and electronic applications. The applications of hybrids nanostructure are shown as nano generators, chemical sensors, photo voltaic, field emission devices, sensitive biological and efficient energy conversion and storage devices [36-39]. Graphene containing the weakly bonded layers of two dimensional hexagonally arranged carbon atoms held together by strong triangular covalent σ-bonds of the sp^2-hybridized orbitals can allow us to transfer the grown inorganic semiconductor nanostructures or films onto the other arbitrary substrates such as glass, metal, and plastic easily.

In view of the significantly enhanced properties and applications of other wide band gap semiconductors coupled with graphene, a wide-band-gap semiconductor β-Ga_2O_3 has been synthesized. In sight of the attractive features of the chemically and thermally stable oxide semiconductor having large direct band gap, the β-Ga_2O_3 can be regarded as a conventional n-type oxide semiconductor with large band-gap of 4.5-5.0 eV [40-42]. Its unique monoclinic lattice (known as β-gallium structure) leads to anisotropy in the optical and electrical properties. For the growth of high band gap inorganic semiconductor on graphene, the most common method used is vapor-phase technique such as metal-organic vapor-phase epitaxy [43, 44]. Several compounds and hybrids has also been synthesized using different methods with graphene using high band gap semiconductors such as graphene-ZnO composites [45, 46], graphene-$ZnGa_2O_4$ complexes [47], graphene-SiC hybrids [48, 49] etc. These reported methods require longer time, accuracy and are costly. Not only time and cost but also the energy required to carry out such reactions can be saved with the MW irradiation route of syntheses.

The MW-assisted method have several advantages as shorter reaction times, environmentally friendly and energy saving technique, uniform distribution of energy inside sample, better reproducibility, excellent control over experimental parameters etc. Here, we introduce a convenient MW-assisted exfoliation method to synthesize 3D β-Ga_2O_3@GNSs hybrids at a lower temperature and ambient pressure. To the best of our knowledge so far, there is no report available on the catalyst free growth of such Ga-based compound materials on GNSs by a MW irradiation method. MW irradiation provides heating the reaction mixture rapidly and homogenously. Therefore, they open up new options for energy and cost saving approaches towards 3D hybrids nanostructure production. This MW irradiation method seems to be a promising method to grow Ga_2O_3 inorganic semiconductors oxide on GNSs with superior controllability in terms of growth rates and structure dimensions. Also, this MW irradiation method is very attractive for large-scale synthesis of such unique 3D hybrids. The synthesized 3D nanomaterial shows significant band gap reducing properties.

Experimental Section

Synthesis of 3D β-Ga_2O_3@GNSs hybrids

First, the starting material graphite oxide (GO) was synthesized by modified Staudenmaier method [50]. In a typical synthesis route for 3D β-Ga_2O_3@GNSs hybrids, GO dried powder (1.2 g) and gallium acetylacetonate ($Ga(C_5H_7O_2)_3$) powder (0.1 g) were added in ethanol (C_2H_5OH) (30 mL). The solution was then sonicated (5 min) and magnetically stirred (10 min) for homogeneous dispersion. During the stirring process, 2 ml NH_4OH (0.5M) was added drop wise in the stirring solution. After stirring for 10 min, the solution was washed with DI water and dried at 30 ^oC. The dried powder were placed in quartz cup and irradiated with MW power (P = 800 and 900 Watt) and for different irradiation time (t = 1, 2 and 3 min). By a few trial experiments, it was found that a 3 min exposure time and 900 W was enough to ensure the completion of the reaction for the growth of 3D β-Ga_2O_3@GNSs hybrids. During the MW irradiation, samples suddenly burned in the form of plasma and converted into black, highly porous materials. After MW irradiation at above power and time, the black porous materials were collected and characterized for structural and morphological analysis.

Materials characterization

The microstructure and morphology of the as-synthesized 3D β-Ga_2O_3@GNSs hybrids were analyzed using X-ray diffraction (XRD, D/MAX-2500/PC; Rigaku Co., Tokyo, Japan), scanning electron microscope (Philips XL 20) and transmission electron microscope (TEM, FEI Tecnai G20, FEI Company, USA). The elemental compositions and defect information of the synthesized materials were analyzed using an X-ray photoelectron spectroscopy (XPS, Axis Ultra, Kratos Analytical Ltd, England) and Raman spectroscopy, respectively. Whereas the optical absorption properties were investigated using a UV-visible diffuse reflectance spectrophotometer (U-41000; HITACHI, Tokyo, Japan). Band gap energies of the Ga_2O_3 and 3D β-Ga_2O_3@GNSs hybrids were calculated by analysis of the Tauc-plots. Room-temperature PL measurement of the powder samples were recorded with a Shimadzu RF-5301PC spectrofluoro-photometer using an excitation wavelength of 250 nm.

Results and discussion

Synthesis scheme of the 3D β-Ga_2O_3@GNSs hybrids are depicted schematically in Figure 1. During MW irradiation process, two different phenomena occur simultaneously. The first is MW induced exfoliation and conversion of GO into few layers GNSs. This exfoliation shows the presence of gaseous products into GO, which

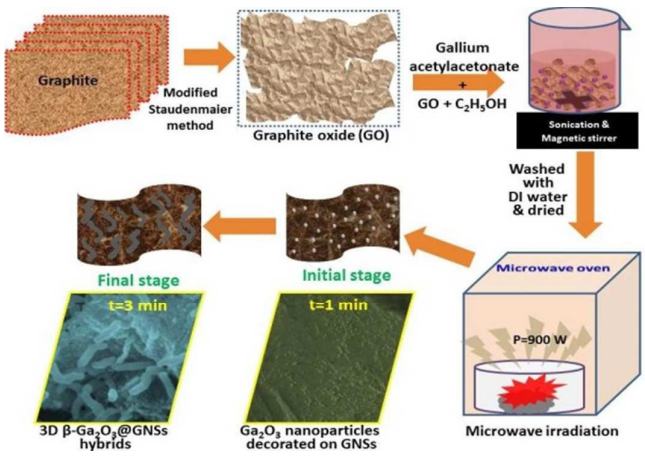

Figure 1. Schematic representation of synthesis of 3D β-Ga_2O_3@GNSs hybrids.

releases in the form of gases (CO_2,CO etc.) resulting in further expansion along the c-axis of the GNSs. The small amount of NH_4OH, reacts with oxygen moieties, carboxyl, hydroxyl, and carbonyl groups of the graphene oxide surfaces and grafts amine groups on it. The formation of β-Ga_2O_3 NWs is initiated from the decomposition of gallium acetylacetonate compound under MW irradiation, resulting in generation of Ga_2O_3 nanoparticles. The complete formation of 3D β-Ga_2O_3@GNSs hybrids takes place when the irradiation power and irradiation time was set at 900 W for 3 min, respectively. The Ga_2O_3 nanoparticles formed and anchored on GNSs induce the growth of β-Ga_2O_3 NWs. The Ga is a metal element, while the GNSs is highly conducting, so the former is more reductive, and is easily get oxygen from the GNSs surface (oxygen containing functional group) to form Ga_2O_3 NWs.

The crystal structure and crystalline phase analysis of the as-synthesized powder materials was characterized by X-ray diffraction (XRD). A characteristic diffraction single and broad peak (002) at 2θ = 10° (Fig. 2a) clearly demonstrates the formation of GO. Inset of

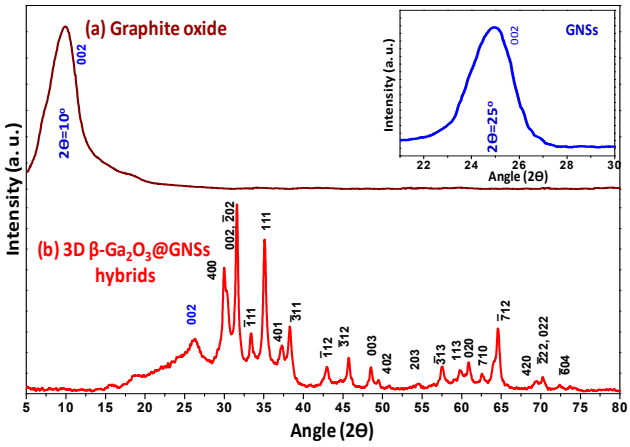

Figure 2. XRD patterns of (a) graphite oxide and (b) 3D β-Ga_2O_3@GNSs hybrids. Inset shows the XRD of GNSs after reduction of GO through MW irradiation.

Figure 2a shows the XRD of GNSs after the reduction and exfoliation of GO through MW irradiation. It clearly shows the shifting of (002) peak from 2θ= 10° to 25° from GO to GNSs and also shows the peak broadening in the GNSs which represents that GNSs have few layer characteristic. The XRD pattern of the as-synthesized 3D β-Ga_2O_3@GNSs hybrids, which was collected after 3 min of MW irradiation at 900W (Figure 2b) match perfectly with the reported β-Ga_2O_3 structure [51]. The XRD pattern of as-synthesized 3D β-Ga_2O_3@GNSs hybrids shows the diffraction peaks at 2θ values of 30.1°, 31.6°, 33.4°, 35.2°, 37.4°, 38.4°, 43.1°, 45.4°, 48.4°, 49.6°, 54.6°, 57.6°, 59.9°, 60.9°, 62.7°, 64.7°, 69.4°, 70.3° and 72.4° can be indexed to (400), $(002, \bar{2}02)$, $(\bar{1}11)$, (111), (401), $(\bar{3}11)$, $(\bar{1}12)$, $(\bar{3}12)$, (003), (402), (203), $(\bar{3}13)$, (113), (020), (710), $(\bar{7}12)$, (420), $(\bar{2}22, 022)$ and $(\bar{6}04)$, respectively to monoclinic structure of Ga_2O_3 with cell constants of *a* = 12.21 Å, *b* = 3.03 Å, *c* = 5.79Å, and β(angle) = 103.83°, (JCPDS file No. 87-1901). We noticed that the relative intensities of the diffraction peak exhibit significance difference between the present pattern and the standard pattern of β-Ga_2O_3 phase as given in JCPDS file (JCPDS file No. 87-1901). In JCPDS file (101) is the first maxima and $(002, \bar{2}02)$ is the second maxima but in our XRD pattern, maximum intensity containing peak is $(002, \bar{2}02)$, which is attributed to preferential growth of worm in this particular direction. No peak associated with the other crystalline forms of the gallium oxides was detected in the pattern. The sharp diffraction peaks also reveal that the as-synthesized β-Ga_2O_3 NWs on GNSs possess a highly crystalline characteristics. The one broad and single peak at 2θ = 26.25° corresponds to (002) plane of graphene due to the GNSs since GO has been effectively reduced and converted into GNSs during MW irradiation [52].

To analyze the changes in surface morphology of hybrids during the synthesis process, SEM micrographs of the GO, exfoliated GNSs and 3D β-Ga_2O_3@GNSs hybrids are shown in Figure 3. Figure 3a shows the agglomerated structure with parallel flacks. After MW exfoliation, these GO gets converted into GNSs as shown in Figure 3b. These GNSs have several micron size lateral graphene sheets with wrinkles on its surfaces. The surface morphology of as-synthesized 3D β-Ga_2O_3@GNSs is shown in Figure 3c, d. SEM observations represents the 3D β-Ga_2O_3@GNSs hybrids with nearly vertical emerging β-Ga_2O_3 NWs on the surfaces of GNSs and later its shows bended morphology. Figure 3c, d shows that β-Ga_2O_3 NWs with low density are grown on GNSs and distributed at the a distance of ~500 nm to 1μm on GNSs. Figure 3c of SEM micrograph shows that the whole GNSs contains 1D β-Ga_2O_3 NWs and standing on 2D GNSs in different directions. Figure 3d shows that the Ga_2O_3 nanoparticles are attached on the graphene surfaces. The high resolution SEM micrograph shown in Figure 3d indicates that the NWs are firmly anchored on the graphene surface, and graphene providing the support to the NWs. We can see that the as synthesized β-Ga_2O_3 NWs are not grown vertical on GNSs surfaces and possess bended structure which looks like earthworm on graphene surfaces. The β-Ga_2O_3 NWs emerge out from the graphene surfaces and show the supporting platform for these NWs. The average diameter and length of the NWs are 200 nm and ~1 μm, respectively.

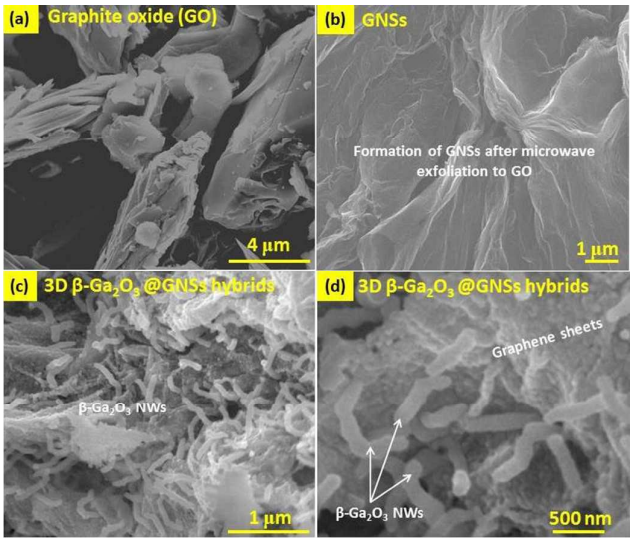

Figure 3. SEM micrographs of (a) graphite oxide, (b) MW exfoliated GNSs and (c, d) 3D β-Ga_2O_3@GNSs hybrids (P = 900 W, t = 3 min).

On the basis of SEM micrographs we found that the different irradiation power and irradiation time have effect on the morphology as shown in Figure 4. When the experiment was conducted for same MW irradiation power (900 W) at different irradiation time (t = 1 min) then β-Ga_2O_3 nanoparticles were decorated on the GNSs surfaces and having diameters 50-80 nm (Fig. 4a). After increasing irradiation time (1 min < t < 2 min), we found that these β-Ga_2O_3 nanoparticles decorated nanoparticles start to agglomerate into larger size nanoparticles. These agglomerated nanoparticles (inside circles) have diameter in the range 100-200 nm (Fig. 4b). For longer MW irradiation time (t = 2 min) we found small NWs like structure on GNSs having lengths 400-600 nm and some β-Ga_2O_3 nanoparticles can be seen on the graphene surfaces (Fig. 4c). This partial growth of NWs and particles on the graphene surfaces suggest that this MW irradiation time is not sufficient for the growth of Ga_2O_3 nanoparticles. Due to this reason Ga_2O_3 nanoparticles could not grow as NWs.

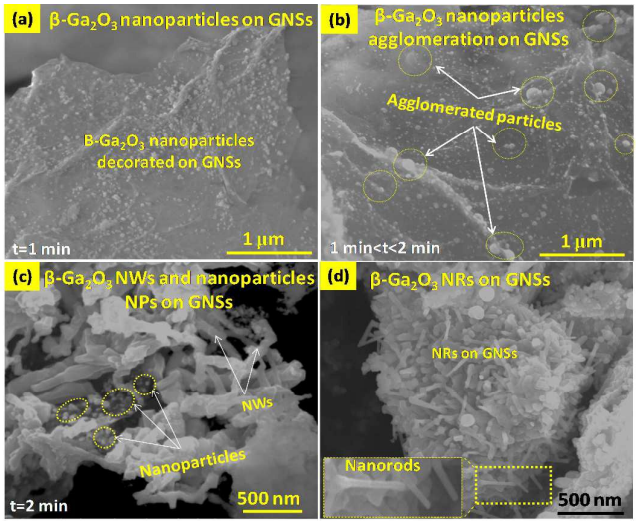

Figure 4. SEM micrographs of (a) Ga_2O_3 nanoparticles at GNSs (P=900 W, t=1 min), (b) β-Ga_2O_3 NWs at GNSs (P=900 W, t=2 min) and (c) β-Ga_2O_3 NRs at GNSs (P=800W, t=3 min).

The less MW irradiation power (P = 800 W, t = 3 min) produces sub-micrometer sized irregularly shaped particles and short nanorods (NRs) with length of 300-500 nm on the GNSs (Fig. 4d). Figure 4d shows the low-magnification SEM image of as-synthesized product and one can clearly see that the large-yield Ga_2O_3 NRs like morphology are randomly grown on the GNSs. However, the majority of the NRs comprised of different length, agglomerates morphology with random growth. Occasionally, small amount of nano needle like Ga_2O_3 NRs can also be found. The structural variations in as synthesized hybrids (nanoparticles, NWs and NRs with GNSs) with respect to MW irradiation power and irradiation time are summarized in Table 1.

On the basis of above observation we can conclude that length of NWs on GNSs increases with the irradiation power with sufficient exposure time for the in-situ chemical reaction for the growth. The β-Ga_2O_3 NWs grown at low irradiation time shows incomplete formation of 1D nanostructure and the structure is dominated by both Ga_2O_3 NWs as well as Ga_2O_3 nanoparticles (Fig. 4c). Such type of structures seems to diminish with the increase in irradiation power. It is speculated that the increase of irradiation time as well irradiation power of MW oven helps to promote the growth Ga_2O_3 NWs on the GNSs and complete formation of 3D β-Ga_2O_3@GNSs hybrids. When the irradiation time is increased (t = 1 min to 3 min) while keeping the irradiation power at the 900 W, the grown structures are basically dominated by the Ga_2O_3 NWs. On the other hand, when the irradiation time is increased while keeping the irradiation power at the 800 W, the Ga_2O_3 NRs structure seems to dominate where their NRs and faceted particles arrangements are coexisting in the nanostructure formation.

S. No.	MW irradiation		Structural variation in hybrids
	Time (t) (Min)	Power (P) (Watt)	
1.	1	900	β-Ga_2O_3 nanoparticles anchoring on GNSs (diameter: 50-80 nm)
2.	2	900	β-Ga_2O_3 NWs and nanoparticles on the GNSs (length ~400-600 nm)
3.	3	900	Growth of β-Ga_2O_3 NWs on the GNSs and complete formation of 3D β-Ga_2O_3@GNSs (length ~ 1 μm)
4.	3	800	β-Ga_2O_3 NRs formations on GNSs (length ~ 200-400 nm)

Table 1. Structural growth variations with MW irradiation power and time

Figure 5a is a typical TEM image of β-Ga_2O_3 NWs, which were grown on GNSs at 900 W for 3 min. This grown morphology shows not completely straight but bended structural β-Ga_2O_3 NWs on GNSs. A high-resolution TEM (HR-TEM) image has been taken from

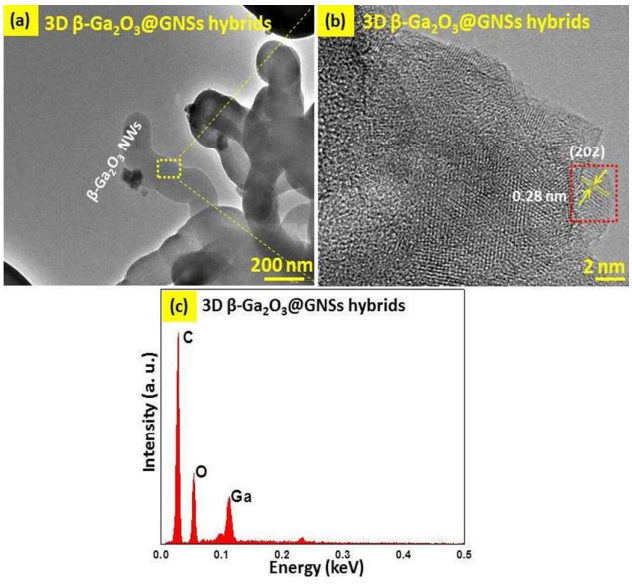

Figure 5. (a) TEM (b) HR-TEM and (c) EDS pattern of 3D β-Ga_2O_3@GNSs hybrids.

NWs as shown in Figure 5b. This HR-TEM image gives further evidence of crystalline ordering within the walls of the β-Ga_2O_3 NWs. Also, indicates the crystalline planes which clearly-resolved interplaner lattices spacing of different plains. The lattice spacing is approximately 0.28 nm corresponding to the distance between $(\bar{2}02)$ planes of β-Ga_2O_3 NWs [53]. Figure 5c shows the energy dispersive spectroscopy (EDS) spectrum of 3D β-Ga_2O_3@GNSs hybrids. The EDS data shows C, Ga and O were the only elements detected, indicating that hybrids have lower Ga content. Based on the obtained results, the atomic weight percentages of C, Ga and O were 81.83, 7.21 and 10.95, respectively. EDX analysis showed that the as-synthesized 3D β-Ga_2O_3@GNSs had an overall Ga:O ratio 1:1.6 close to the expected 1:1.5 for Ga_2O_3. The existence of Ga and O with an approximate ratio of 2:3 implies its stoichiometry.

Raman spectroscopy is a convenient and powerful tool to study structural characteristics of materials and used to distinguish the order and disorder/defect structures in hybridized carbon. The Raman characteristic peaks of GNSs and 3D β-Ga_2O_3@GNSs hybrids are shown in Figure 6. There exist two strong peaks centred at 1351 cm^{-1} (D-band) and 1586 cm^{-1} (G-band) in both samples. The peak at

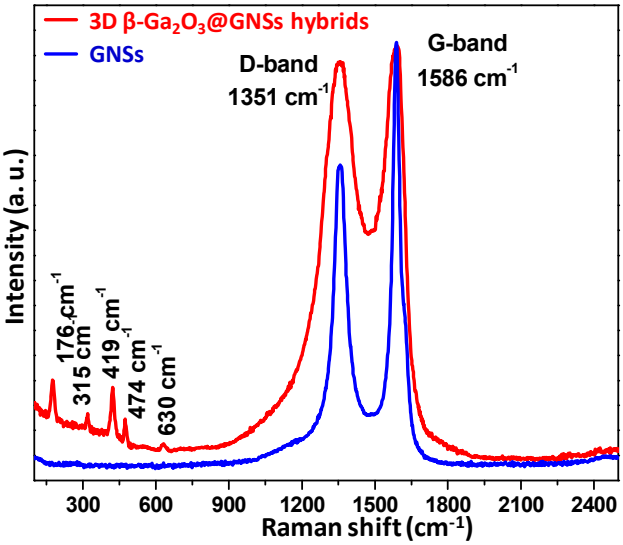

Figure 6. Raman spectra of GNSs and 3D β-Ga_2O_3@GNSs hybrids.

1351 cm^{-1} corresponds to the Raman-inactive A_{1g} in-plane breathing vibration mode, and is related to the defects and disorders in structures in carbonaceous solids. The G-band assigned to the Raman-active E_{2g} mode corresponds to the stretching vibration in the basal-plane of graphite, and generally used to identify well-ordered GNSs. The D-band is connected with the defects and disorder in the hexagonal graphitic layers, while the G-band is associated with the Raman-active E_{2g} mode induced by the presence of sp^2 carbon-type structures [54]. The intensity ratio of D-band and G-band (I_D/I_G) is used to estimate the graphitization quality of graphene based materials. The I_D/I_G value for GNSs and 3D β-Ga_2O_3@GNSs hybrids was found to be 0.72 and 0.97, respectively. This represents more plane defects in the β-Ga_2O_3@GNSs hybrids as compared to GNSs due to the growth of β-Ga_2O_3 NWs. Also, after formation of 3D β-Ga_2O_3@GNSs hybrids, the D and G band peaks gets broadened the FWHM value is found to be 111 cm^{-1} and 83 cm^{-1} for D band and G-band respectively. However, in the case of GNSs, the FWHM appears as 48 cm^{-1} and 35 cm^{-1} corresponding to D and G-band respectively. The 3D β-Ga_2O_3@GNSs hybrids exhibits five peaks at lower Raman shift side at 176, 315, 419, 474 and 630 cm^{-1}, which match well with the Raman spectrum reported for β-Ga_2O_3 phase [55].

To determine the elemental presence in as synthesized 3D β-Ga_2O_3@GNSs hybrids, the X-ray photoelectron spectroscopy (XPS) was performed. Figure 7a displays a full scan in the energy ranging from 0 to 1200 eV and the peaks corresponding to C 1s, O 1s, Ga 2p, Ga 3p, Ga 3s and Ga 3d as well as the O KLL and Ga LMM auger lines can be observed [56]. In Figure 7b, the gallium core levels Ga ($2p_{3/2}$)

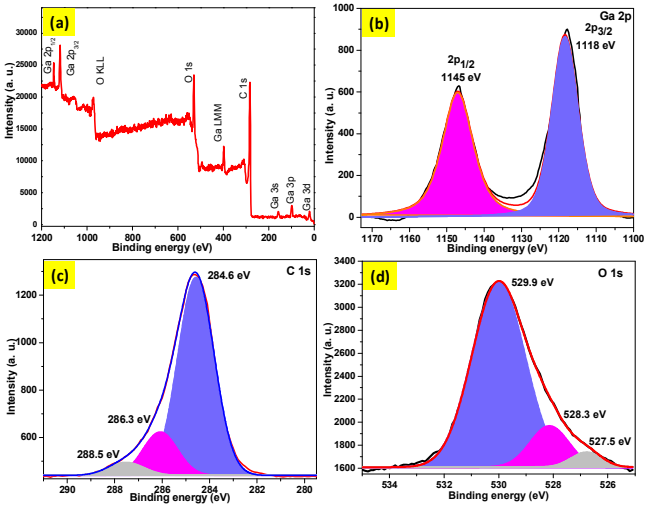

Figure 7. XPS spectra of 3D β-Ga_2O_3@GNSs hybrids. (a) Complete survey (b) Ga 2p spectra (c) C 1s spectra and (d) O 1s spectra.

and Ga ($2p_{1/2}$) are observed at 1118 eV and 1145 eV, respectively, with a peak-to-peak separation of 27eV which confirms the formation of β-Ga_2O_3 in as synthesized 3D β-Ga_2O_3@GNSs hybrids [57]. Figure 7c shows the C 1s peak which can be deconvoluted into three peaks centred at 284.6, 286.3 and 288.5 eV, corresponding to the binding energies of the C=C (sp^2), C-O and C= O bonds [58]. The C=C bond (sp^2) is found to be the main contributor indicating the as-prepared material to be GNSs. Figure 7d presents the O1s peak located at 529.9 eV, which can be divided into two separate peaks located at 528.3 and 527.5 eV by deconvolution fitting. The key peak located at 530.8eVcan be assigned to the Ga-O bonding and the other weak peak at 532.2eV owing to the C/O or OH adsorbed species on the surface. From the XPS spectra, the ratio of Ga and O is estimated to be about 1:1.6; the concentration of O is a little higher than normal chemical composition possibly due to the existence of surface adsorbed oxygen functionalities on GNSs. This stoichiometry has been also confirmed by EDS spectra in Figure 5. Therefore, the XPS results confirm that the synthesized hybrids contains β-Ga_2O_3 phase with stoichiometry ratio of ~ 2:3.

UV-visible absorption spectroscopy was used as a tool to determine the band gap energy of 3D β-Ga_2O_3@GNSs hybrids. The

optical band gap for a semiconductor near the absorption band edge can be estimated from the following equation known as the Tauc plot [59].

$$(\alpha h\nu) \propto (h\nu - E_g)^n$$

Where α is the optical absorption coefficient, $h\nu$ is the energy of the incident photon, E_g the optical band and n=½ and 2 correspond to direct allowed transition semiconductor and indirect allowed transition semiconductor respectively. The inset of figure 8 shows the Tauc plot of $(\alpha h\nu)^2$ versus energy of light photon ($h\nu$). By extrapolating the linear part of $(\alpha h\nu)^2$ curve, the direct band gap was determined for β-Ga_2O_3 and 3D β-Ga_2O_3@GNSs hybrids. The band gap energy for the synthesized 3D β-Ga_2O_3@GNSs hybrids is 4.48 eV, corresponds to an optical absorption edge of 264 nm estimated from its UV-visible absorption spectrum in Figure 8. Also the band gap energy for β-Ga_2O_3 nanostructure is 4.94 eV, corresponds to an optical absorption edge of 255 nm. With the formation of 3D β-Ga_2O_3@GNss hybrids, E_g decreases from 4.94 to 4.48 eV which shows the red shift of E_g and could be associated with the structural evolution, i.e., the NWs formations on GNSs. The surfaces of GNSs consisting β-Ga_2O_3 rich phase of self-assembled NWs on its surface intensively absorb light near the UV region. There are several reports regarding the red shift of E_g by a metallic particles or clusters [60].

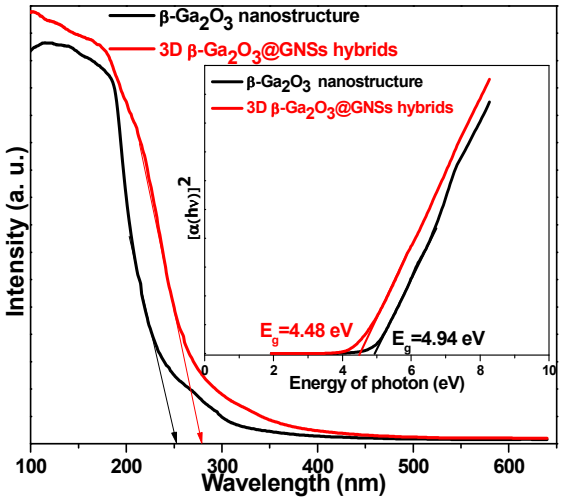

Figure 8. UV visible spectra of β-Ga_2O_3 and 3D β-Ga_2O_3@GNSs hybrids.

The optical properties of as-synthesized samples were also investigated by photoluminescence (PL) measurement. The PL spectra provide separation and recombination information for the photo induced electrons and holes in the material [61]. Figure 9 shows the room temperature PL spectra of β-Ga2O3 and 3D β-Ga_2O_3@GNSs hybrids with UV florescent light excitation wavelength of 250 nm. For the as-prepared β-Ga_2O_3 nanoparticles, two luminescence peaks at 355 and 445 nm are seen. The intensity of the peak at 355 nm is considerably very weak than that of the peak at 445 nm. This weak peak at 355 nm is assigned to the recombinations due to self-trapped excitation [61-63]. The stronger luminescence emission peak centered at 445 nm can be attributed to the surface defects and oxygen vacancies in the Ga_2O_3 nanostructure lattice. This emission peak can be assigned to the electrons that are excited and recombined on the surface of the Ga_2O_3 nanoparticles. These combine radiatively to emit a blue photon. The blue emission occurring in β -Ga2O3 has been observed by other researchers also [28, 29, 63-66]. It originates mainly from the recombination of an electron on a donor formed by oxygen vacancies and a hole on an acceptor formed by metal vacancies, the blue photon is emitted via the radiative recombination process [61, 64, 67]. In the case of 3D β-Ga_2O_3@GNSs hybrids, the 435 nm peaks shows the decreased emission intensity as compared to Ga_2O_3 nanostructure with slight broadening. The decreased intensity of 3D β-Ga_2O_3@GNSs hybrids show a blue shift of ~10 nm compared with the peak 445 nm of β-Ga_2O_3 nanostructure. The decreased intensity is due to lower recombination of photo-generated electron–hole pairs induced by the charge transfer between the GNSs and the β-Ga_2O_3 nanostructure. It is known that Ga_2O_3 nanostructure is an electron donor and the carbon materials such as GNSs are known to be good electron acceptors [68, 69]. Thus, the synergistic effects between these two, GNSs and the β-Ga_2O_3 nanostructure would effectively reduce the recombination of the photo generated electron–hole pairs and this 435 nm peak gets suppressed. This indicates that the 3D β-Ga_2O_3-GNSs hybrids has a lower recombination rate of electrons and holes under UV light irradiation, which is mainly due to the fact that the electrons are excited from the valence band of Ga_2O_3 to the conduction band and then transferred to GNSs, preventing a direct recombination of the electrons and holes. The observed slight blue-shifting (10 nm) in β-Ga_2O_3@GNSs hybrids is consistent with the presence of the defects [62, 63]. Also this 435 nm decreased intensity in 3D β-Ga_2O_3@GNSs hybrid tends towards quenching phenomena [46].

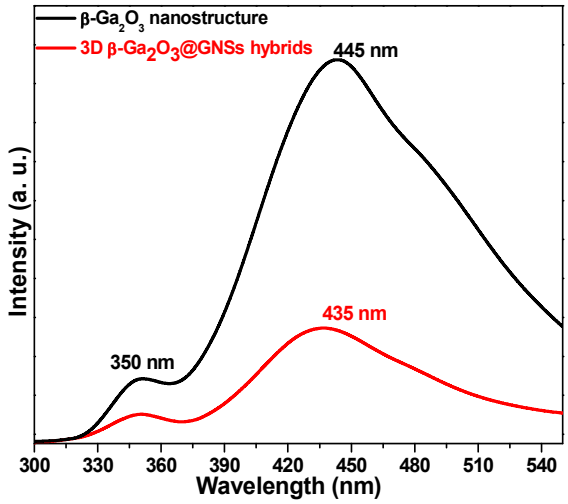

Figure 9. Photoluminescence spectra of β-Ga_2O_3 and 3D β-Ga_2O_3@GNSs hybrids.

Mechanism for the growth of 3D β-Ga_2O_3@GNSs hybrids

The schematic diagram in Figure 10 depicts the stepwise creation of the 3D β-Ga_2O_3@GNSs hybrids. On the basis of obtained information, it can be concluded that the two parameters irradiation time and power played important roles in the formation of different nanostructures NRs and NWs on GNSs surfaces. The experimental results imply that the morphology of as-synthesized

3D β-Ga_2O_3@GNSs hybrids is very sensitive and the key parameters governing the reaction conditions are irradiation power (900 W) and time (3 min). Reaction time is usually known to be an important influencing factor for morphological control [70]. The MW irradiation induced chemical and thermal reaction at molecular label is responsible for the attachment of nanoparticles on GNSs and growth of NRs and NWs. When MW irradiation is applied on the initial materials, the extraction of GNSs from GO (GO carbonaceous chemicals get combusted evolving some gases) and Ga is decomposed from its host material ($Ga(C_5H_7O_2)_3$). In this process, a significant amount of heat is released, and the local temperature of the sample becomes much higher than the actual room temperature. The GNSs surface with good MW absorptivity decomposes the nearby Ga salt particles to promote the instantaneous formation of Ga oxide nanoparticles, decorating the GNSs surfaces within minutes of MW exposure. Also, GNSs have oxygen containing functionalities (epoxy, hydroxyl, carbocyclic and carboxyl etc.) on its surface and edges that become negatively charged. The positive Ga ions interact with the functional groups via

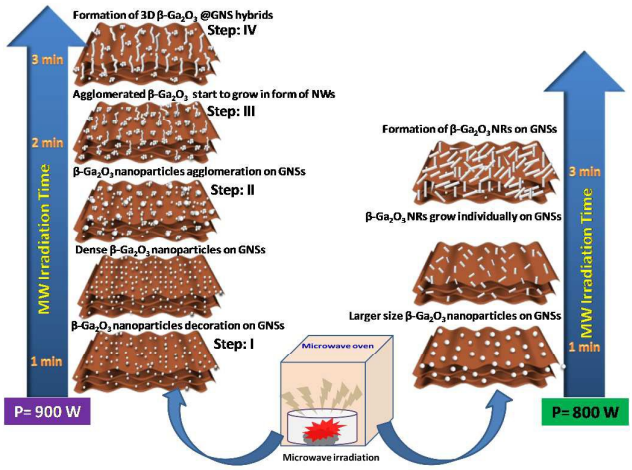

Figure 10. Schematic mechanism for the growth of 3D β-Ga_2O_3@GNSs hybrids.

electrostatic attraction and combined with these functionalities. These Ga ions attached with the surface of GNSs, get oxidized and convert into β-Ga_2O_3 nanoparticles which is the most stable phase by absorbing the thermal energy from MW irradiation. The decorated β-Ga_2O_3 nanoparticles on GNSs surfaces at 900 W and reaction time 1 min is shown in Figure 10 (Step: I). It was found that the high exposure of MW irradiation could result in the formation of more nanoparticles on the GNS surfaces (Step: II). The continuous MW irradiation seemed to have enhanced the local heating and initially formed β-Ga_2O_3 nanoparticles to yield agglomerated larger nanoparticles (Step: III). The decorated β-Ga_2O_3 nanoparticles start to assemble for longer irradiation time acquiring high energy from MW. In the subsequent process, to minimize the surface free energy of the system, the decorated β-Ga_2O_3 nanoparticles continuously assembles into cluster forms. The MW irradiation with high heating rate and homogeneous volumetric heating felicitously provides a favourite condition for nucleation and growth. The continuous MW irradiation only 3 min induces speedy nucleation and growth of NWs in one direction from agglomerated β-Ga_2O_3 clusters on the GNSs surfaces (Step: IV). The β-Ga_2O_3 NWs are in low density on GNSs surface because the agglomeration of β-Ga_2O_3 nanoparticles provides spaces at certain distances (500 nm - 1 µm) after the nucleation and growth. Further in the formation of larger size NWs (~ 1 µm), more nuclei would readily aggregate. Also some agglomerated β-Ga_2O_3 nanoparticles are left on GNSs surface due to improper nucleation for the growth of β-Ga_2O_3 NWs (Step-IV). At lower irradiation power (800 W), β-Ga_2O_3 nanoparticles were not able to agglomerate on the GNSs surfaces and start to nucleate before agglomeration. These individual β-Ga_2O_3 nanoparticle forms smaller size NRs and also, initially individual nucleated particles does not get sufficient energy and are kinetically not favoured for continuous 1D growth and stops their straight growth after desired growth in the form of short length NRs. These grown β-Ga_2O_3 NRs on GNSs are dense because all individual β-Ga_2O_3 nanoparticles are responsible for the formation of NRs on the GNSs.

Conclusions

We have employed a simple, eco-friendly, fast and cost effective MW irradiation method. The reaction involves 1-3 min of MW irradiation for the formation of 3D β-Ga_2O_3@GNSs hybrids under atmospheric pressure to produce NWs of β-Ga_2O_3 on GNSs with diameters of 200 nm and lengths up to ~1 µm. This study also successfully provide a mechanism to synthesize β-Ga_2O_3 NRs on GNS and Ga_2O_3 nanoparticles decorated GNSs structure by a simple and low-cost MW irradiation. Raman spectra clearly give the evidence that the as synthesized 3D β-Ga_2O_3@GNSs hybrids have more defective structure due to 1D NWs grown on GNSs. The 3D β-Ga_2O_3@GNSs hybrids show band gap reducing phenomena and have lower band gap (4.48 eV) as comparison to pristine β-Ga_2O_3 (4.94 ev) structures. By choosing appropriate semiconducting metal oxides, we expect that the present method can be extended to synthesize others 3D hybrids comprising 1D nanowires, nanorods or nanoworms like structure on graphene sheets.

Acknowledgements

RK, ARV and SAM would like to acknowledge CNPq and FAPESP (Brazil) for financial support.

Notes and references

1. X. Xu, M. Lei, K. Huang, C. Liang, J. C. Xu, Z. C. Shangguan, Q. X. Yuan, L. H. Ma, Y. X. Du, D. Y. Fan, H. J. Yang, Y. G. Wang and W. H. Tang, *Journal of Alloys and Compounds*, 2015, **623**, 24-28.
2. G.-L. Chai, C.-S. Lin and W.-D. Cheng, *Journal of Materials Chemistry*, 2012, **22**, 7708-7711.
3. G.-L. Chai, C.-S. Lin and W.-D. Cheng, *Journal of Materials Chemistry*, 2011, **21**, 17071-17076.
4. S. Strite and H. Morkoç, *Journal of Vacuum Science & Technology B*, 1992, **10**, 1237-1266.
5. Y. Masubuchi, R. Yamaoka, T. Motohashi, K. Kirihara, W. Lee, K. Watanabe, T. Sekiguchi and S. Kikkawa, *Journal of Crystal Growth*, 2011, **337**, 87-92.

6. M. Passlack, E. F. Schubert, W. S. Hobson, M. Hong, N. Moriya, S. N. G. Chu, K. Konstadinidis, J. P. Mannaerts, M. L. Schnoes and G. J. Zydzik, *Journal of Applied Physics*, 1995, **77**, 686-693.
7. C.-C. Hu and H. Teng, *The Journal of Physical Chemistry C*, 2010, **114**, 20100-20106.
8. M. Kerlau, P. Reichel, N. Bârsan, U. Weimar, S. Delsarte-Guéguen and O. Merdrignac-Conanec, *Sensors and Actuators B: Chemical*, 2007, **122**, 14-19.
9. S. Nakamura, *Science*, 1998, **281**, 956-961.
10. M. Kerlau, O. Merdrignac-Conanec, P. Reichel, N. Bârsan and U. Weimar, *Sensors and Actuators B: Chemical*, 2006, **115**, 4-11.
11. J. S. Wright, W. Lim, B. P. Gila, S. J. Pearton, J. L. Johnson, A. Ural and F. Ren, *Sensors and Actuators B: Chemical*, 2009, **140**, 196-199.
12. M. Higashiwaki, K. Sasaki, A. Kuramata, T. Masui and S. Yamakoshi, *physica status solidi (a)*, 2014, **211**, 21-26.
13. D.-H. Lien, Y.-H. Hsiao, S.-G. Yang, M.-L. Tsai, T.-C. Wei, S.-C. Lee and J.-H. He, *Nano Energy*, 2015, **11**, 104-109.
14. K. Matsuzaki, H. Hiramatsu, K. Nomura, H. Yanagi, T. Kamiya, M. Hirano and H. Hosono, *Thin Solid Films*, 2006, **496**, 37-41.
15. F. Zhu, Z. Yang, W. Zhou and Y. Zhang, *Applied Surface Science*, 2006, **252**, 7930-7933.
16. X. Wang, Q. Xu, M. Li, S. Shen, X. Wang, Y. Wang, Z. Feng, J. Shi, H. Han and C. Li, *Angewandte Chemie International Edition*, 2012, **51**, 13089-13092.
17. S. Jin, X. Wang, X. Wang, M. Ju, S. Shen, W. Liang, Y. Zhao, Z. Feng, H. Y. Playford, R. I. Walton and C. Li, *The Journal of Physical Chemistry C*, 2015, **119**, 18221-18228.
18. X. Li, X. Zhen, S. Meng, J. Xian, Y. Shao, X. Fu and D. Li, *Environmental Science & Technology*, 2013, **47**, 9911-9917.
19. W. Zhang, B. S. Naidu, J. Z. Ou, A. P. O'Mullane, A. F. Chrimes, B. J. Carey, Y. Wang, S.-Y. Tang, V. Sivan, A. Mitchell, S. K. Bhargava and K. Kalantar-zadeh, *ACS Applied Materials & Interfaces*, 2015, **7**, 1943-1948.
20. L. Mazeina, F. K. Perkins, V. M. Bermudez, S. P. Arnold and S. M. Prokes, *Langmuir*, 2010, **26**, 13722-13726.
21. L. Mazeina, Y. N. Picard, S. I. Maximenko, F. K. Perkins, E. R. Glaser, M. E. Twigg, J. A. Freitas and S. M. Prokes, *Crystal Growth & Design*, 2009, **9**, 4471-4479.
22. C.-H. Hsieh, L.-J. Chou, G.-R. Lin, Y. Bando and D. Golberg, *Nano Letters*, 2008, **8**, 3081-3085.
23. T. Wang, S. S. Farvid, M. Abulikemu and P. V. Radovanovic, *Journal of the American Chemical Society*, 2010, **132**, 9250-9252.
24. P.-H. Chen, C.-H. Hsieh, S.-Y. Chen, C.-H. Wu, Y.-J. Wu, L.-J. Chou and L.-J. Chen, *Nano Letters*, 2010, **10**, 3267-3271.
25. J. Q. Hu, Q. Li, X. M. Meng, C. S. Lee and S. T. Lee, *The Journal of Physical Chemistry B*, 2002, **106**, 9536-9539.
26. Y. C. Choi, W. S. Kim, Y. S. Park, S. M. Lee, D. J. Bae, Y. H. Lee, G. S. Park, W. B. Choi, N. S. Lee and J. M. Kim, *Advanced Materials*, 2000, **12**, 746-750.
27. Z. R. Dai, Z. W. Pan and Z. L. Wang, *The Journal of Physical Chemistry B*, 2002, **106**, 902-904.
28. J. Zhang and F. Jiang, *Chemical Physics*, 2003, **289**, 243-249.
29. K. W. Chang and J. J. Wu, *Appl Phys A*, 2003, **76**, 629-631.
30. M. D. Stoller, S. Park, Y. Zhu, J. An and R. S. Ruoff, *Nano Letters*, 2008, **8**, 3498-3502.
31. A. A. Balandin, S. Ghosh, W. Bao, I. Calizo, D. Teweldebrhan, F. Miao and C. N. Lau, *Nano Letters*, 2008, **8**, 902-907.
32. C. Lee, X. Wei, J. W. Kysar and J. Hone, *Science*, 2008, **321**, 385-388.
33. J.-H. Chen, C. Jang, S. Xiao, M. Ishigami and M. S. Fuhrer, *Nat Nano*, 2008, **3**, 206-209.
34. K. I. Bolotin, K. J. Sikes, Z. Jiang, M. Klima, G. Fudenberg, J. Hone, P. Kim and H. L. Stormer, *Solid State Communications*, 2008, **146**, 351-355.
35. N. Gao and X. Fang, *Chemical Reviews*, 2015, **115**, 8294-8343.
36. N. Neeraj, D. W. Virginia, J. A. Travis, J. K. Francis, A. M. Michael, L. M.-W. Rachael, B. Q. Syed, A. F. Jaime, C. H. Sandra, O. N. Luke, G. W. Scott, G. Kurt and Charles R Eddy, Jr., *Applied Physics Express*, 2013, **6**, 061003.
37. K. S. Novoselov, V. I. Falko, L. Colombo, P. R. Gellert, M. G. Schwab and K. Kim, *Nature*, 2012, **490**, 192-200.
38. W. Jie and J. Hao, *Nanoscale*, 2014, **6**, 6346-6362.
39. W. I. Park, C.-H. Lee, J. M. Lee, N.-J. Kim and G.-C. Yi, *Nanoscale*, 2011, **3**, 3522-3533.
40. T. Oshima, T. Okuno and S. Fujita, *Japanese Journal of Applied Physics*, 2007, **46**, 7217.
41. M. Orita, H. Ohta, M. Hirano and H. Hosono, *Applied Physics Letters*, 2000, **77**, 4166-4168.
42. Y. Jia, K. Zeng, J. S. Wallace, J. A. Gardella and U. Singisetti, *Applied Physics Letters*, 2015, **106**, 102107.
43. H. Baek, C.-H. Lee, K. Chung and G.-C. Yi, *Nano Letters*, 2013, **13**, 2782-2785.
44. P. Gupta, A. A. Rahman, N. Hatui, M. R. Gokhale, M. M. Deshmukh and A. Bhattacharya, *Journal of Crystal Growth*, 2013, **372**, 105-108.
45. N. Song, H. Fan and H. Tian, *Applied Surface Science*, 2015, **353**, 580-587.
46. R. Kumar, R. K. Singh, J. Singh, R. S. Tiwari and O. N. Srivastava, *Journal of Alloys and Compounds*, 2012, **526**, 129-134.
47. K. Huang, X. S. Zhao, Y. F. Li, X. Xu, C. Liang, D. Y. Fan, H. J. Yang, R. Zhang, Y. G. Wang and M. Lei, *Materials Research Bulletin*, 2014, **60**, 453-456.
48. K. Zhu, L. Guo, J. Lin, W. Hao, J. Shang, Y. Jia, L. Chen, S. Jin, W. Wang and X. Chen, *Applied Physics Letters*, 2012, **100**, 023113.
49. S. Lin, X. S. Zhao, Y. F. Li, K. Huang, R. X. Jia, C. Liang, X. Xu, Y. F. Zhou, H. Wang, D. Y. Fan, H. J. Yang, R. Zhang, Y. G. Wang and M. Lei, *Materials Letters*, 2014, **132**, 380-383.
50. L. Staudenmaier, *Berichte der deutschen chemischen Gesellschaft*, 1898, **31**, 1481-1487.
51. H.-a. Park, J. H. Choi, K. M. Choi, D. K. Lee and J. K. Kang, *Journal of Materials Chemistry*, 2012, **22**, 5304-5307.
52. R. Kumar, R. K. Singh, P. K. Dubey, D. P. Singh and R. M. Yadav, *ACS Applied Materials & Interfaces*, 2015, **7**, 15042-15051.
53. Y. Su, M. Gao, X. Meng, Y. Chen, Q. Zhou, L. Li and Y. Feng, *Journal of Physics and Chemistry of Solids*, 2009, **70**, 1062-1065.
54. T. Xu, L. Zhang, H. Cheng and Y. Zhu, *Applied Catalysis B: Environmental*, 2011, **101**, 382-387.
55. S. C. Vanithakumari and K. K. Nanda, *Advanced Materials*, 2009, **21**, 3581-3584.
56. X. Feng, Z. Li, W. Mi, Y. Luo and J. Ma, *Materials Science in Semiconductor Processing*, 2015, **34**, 52-57.
57. C. V. Ramana, E. J. Rubio, C. D. Barraza, A. Miranda Gallardo, S. McPeak, S. Kotru and J. T. Grant, *Journal of Applied Physics*, 2014, **115**, 043508.
58. G. Li, Y. Li, H. Liu, Y. Guo, Y. Li and D. Zhu, *Chemical Communications*, 2010, **46**, 3256-3258.
59. H. Jia, H. Xu, Y. Hu, Y. Tang and L. Zhang, *Electrochemistry Communications*, 2007, **9**, 354-360.
60. K. H. Choi and H. C. Kang, *Materials Letters*, 2014, **123**, 160-164.

61. T. Harwig and F. Kellendonk, *Journal of Solid State Chemistry*, 1978, **24**, 255-263.
62. B. Geng, L. Zhang, G. Meng, T. Xie, X. Peng and Y. Lin, *Journal of Crystal Growth*, 2003, **259**, 291-295.
63. H.-S. Qian, P. Gunawan, Y.-X. Zhang, G.-F. Lin, J.-W. Zheng and R. Xu, *Crystal Growth & Design*, 2008, **8**, 1282-1287.
64. C. H. Liang, G. W. Meng, G. Z. Wang, Y. W. Wang, L. D. Zhang and S. Y. Zhang, *Applied Physics Letters*, 2001, **78**, 3202-3204.
65. G. Gundiah, A. Govindaraj and C. N. R. Rao, *Chemical Physics Letters*, 2002, **351**, 189-194.
66. Y. Wang, L. Hou, X. Qin, S. Ma, B. Zhang, H. Gou and F. Gao, *The Journal of Physical Chemistry C*, 2007, **111**, 17506-17511.
67. L. Binet and D. Gourier, *Journal of Physics and Chemistry of Solids*, 1998, **59**, 1241-1249.
68. X.-F. Zhang and Q. Xi, *Carbon*, 2011, **49**, 3842-3850.
69. S. Barja, M. Garnica, J. J. Hinarejos, A. L. Vazquez de Parga, N. Martin and R. Miranda, *Chemical Communications*, 2010, **46**, 8198-8200.
70. G. R. Patzke, Y. Zhou, R. Kontic and F. Conrad, *Angewandte Chemie International Edition*, 2011, **50**, 826-859.